Electrokinetic Insect-Bioinspired Membrane Pumping in a High Aspect Ratio Bio-Microfluidic System

V. K. Narla[1], Dharmendra Tripathi[2*†], D. S. Bhandari[2†]
and O. Anwar Bég[3†]

[1*]Department of Mathematics, GITAM Deemed to be University, Hyderabad-502329, India.
[2]Department of Mathematics, National Institute of Technology Uttarakhand, Srinagar-246174, India.
[3]Multi-Physical Engineering Sciences Group, Salford University, Manchester, UK.

*Corresponding author(s). E-mail(s): dtripathi@nituk.ac.in;
Contributing authors: vknarla@gmail.com;
dsbhandari11@gmail.com; gortoab@gmail.com;
[†]These authors contributed equally to this work.

Abstract

Microscale flows utilizing stimulus-responsive working fluids are finding increasing applications in emerging areas in mechanical, biological and chemical engineering. Motivated by such applications, in the present article, an analytical study of the electrokinetic effect on insect bio-inspired rhythmic pumping is conducted for a high aspect ratio micro-tube. The membrane attached to the wall performs periodic compression and expansion phases during the complete contraction cycle. Thus, the micro-pump transports the fluid owing to wall deformation by virtue of membrane kinematics. Electroosmotic phenomena are simulated with the Poisson-Boltzmann equation. The impact of the membrane shape parameter is retained in the model. The effects of Helmholtz-Smoluchowski velocity (U_{HS}) and reciprocal of electrical double layer thickness (κ) on the pressure distribution, radial and axial velocity distribution, volumetric flow rate pumping characteristic, wall shear stress, and vector field streamline patterns are visualized graphically and interpreted the physical significance. The simulations show that

volumetric flow rate and wall shear stress are elevated for thinner EDL. A boost in wall shear stress accompanies an increment in positive U_{HS} in the vicinity of the membrane. The magnitude of the axial velocity is positive for $U_{HS} = -1$ (positive direction of axial electrical field) whereas negative values are computed for $U_{HS} = 1$ (reversed direction of axial electrical field). The present analysis furnishes some novel insights into membrane-based pumping mechanisms in electroosmotic microfluidics devices relevant to the manipulation of microscale internal flow in bio-medicine, soft robotics and other areas.

1 Introduction

In recent decades, considerable expansion in the area of microfluidics has occurred driven by new emerging applications in bio-inspired technological systems and optimizing biomedical process designs. The resulting bio-microfluidics systems make it possible to miniaturize microfluidics systems on a microchip and are highly efficient and portable, enabling many new operations in bio medicine to be achieved more successfully and with increased manipulation capabilities for deployment. These include sample micro-pumping, bio-chip devices for micromixing, microfluidic-based biomedical separation and concentration, DNA analysis, forensics, disease monitoring etc. In addition, these techniques can be used in bio-logical applications to fabricate bio-mimetic lab-on-a-chip devices (LOC) or bio-micro-electro-mechanical systems (bioMEMS) [1–5] which are becoming increasingly popular in the 21st century.

Ions and ferrites in hemoglobin molecules which arise in physiological fluids allow them to respond to external electrical and magnetic fields. This has led to a new avenue for multi-physical fluid dynamics in which biological fluent media can be treated as naturally smart or intelligent and can be coordinated to respond to a variety of external stimuli. In electrokinetics transport [6] typically, an electric double layer (EDL) is formed near the charged surface (e.g. blood vessel wall, tissue membrane etc) as a charged solid surface comes into contact with an aqueous-based electrolyte (ionic) solution e.g. blood, synovial lubricant, cerebral drugs etc [7–9]. Therefore, when an electric field is imposed, the EDL has induced a bulk fluid flow which is commonly referred to as electroosmotic flow and arises in for example transport in the human eye, cardiovascular flows, kneecap meniscus tribology and other areas. It also constitutes an important mechanism in translocation and fluid motion in trees and plants under capillary forces. Recently, engineers have mobilized a new initiative to mimic this very efficient mechanism in order to enhance

existing microfluidics technologies with optimized external pumping techniques which can very efficiently transport minute amounts of fluids. New electro-biomicrofluidic systems have therefore been manufactured including phase-controlled electrohydrodynamic mixing, electro-fluid diagnostics, bio molecule translocation in protein detection, digital forensic microfluidics platforms in crime scene investigation, electrochemical biosensors for electrokinetic enhanced immune-reaction studies etc. In such systems [10–14], both static and alternating electrical (and magnetic) fields may feature, and with regard to electroosmotic mobility, an important consideration is the zeta potential which constitutes the voltage at the edge of the shearing plane on the surface of electrodes to the bulk medium. Furthermore the performance of such devices is strongly linked to the *ionic conductivity* of working fluids. In parallel with the extensive laboratory-based investigations reported in electro-biomicrofluidics, mathematical and numerical simulations provide a very powerful insight. Many studies have therefore addressed electroosmotic flow (EOF) in a micro-channel and have deployed both Newtonian and non-Newtonian models. A popular approach has been the use of low Reynolds number models and lubrication approximations to simulate the interaction of viscous, electric field and other forces with a variety of geometric channel properties [15–19]. These studies have also utilized many analytical and numerical techniques to accommodate the non linearity of the coupled mathematical models arising including finite element, Lattice Boltzmann, and other solvers. Harnett et al. [20] have examined induced-charge electroosmosis (ICEO) to enhance mixing in microfluidics devices using a finite volume method (FVM) to compute the distribution of the electric field, fluid flow and mass transport through a multi-species liquid. Bég et al. [21] used a combined differential transform method (DTM) with Padé approximate to compute the electrokinetic pumping of ionic solutions in rigid conduits with electrical Hartmann and electrical Reynolds number effects. Pan et al. [22] deployed a Lagrangian smoothed particle hydrodynamics (SPH) code to numerically evaluate the protein ligand binding rates in electroosmotic diffusion in bio molecular enzyme transport with reactive Robin boundary conditions at the charged surfaces. Bég et al. [23] implemented a Chebyschev spectral collocation method to analyze the ionic electrical potential distribution in electroosmotic flow in micro-tubes with electrical source effects. Gogoi [24] applied a molecular dynamics (MD) technique to examine the electroosmotic flows in a nano-channel with variable surface charges.

In recent years bio-microfluidics devices have embraced *bio-inspired* designs. These replicate certain highly efficient mechanisms encountered in nature to enhance the performance of engineering systems to achieve higher efficiency, lower maintenance and self-adaption. Many such mechanisms have been studied including anti-bacterial coatings [25], natural sponge-inspired hetero structured media for bio molecular cleaning [26], internal ciliated surfaces for bio-robotics [27] and multi-tactic micro-organism doping for bio-inspired

fuel cells [28]. In the studies described earlier, exploiting the fundamental principle of electroosmosis for physiological fluid manipulation, the conduits considered (blood vessel, micro-channel etc) have been generally assumed to be rigid i.e. the boundaries are *non-flexible*. This leads to lower efficiency for transportation of bio-fluids. The manipulation of fluid with precise control through a system is one of the most critical aspects of designing efficient channel geometries in bio microfluidics. To improve pumping efficiency of synthesized devices, an alternative bio-inspired mechanism which exploits the compliance (deformability) of the conduit is peristalsis. Peristaltic pumping [29] is a highly efficient mechanism encountered extensively in biology which enables sustained fluid dynamic transport or external locomotion via rhythmic contraction and expansion of a conduit surface, and is achieved with elegant muscle operation. This elongation–contraction is observed in human digestion, swallowing, blood flow etc. In the motion of certain organisms [30] including the sea snail (*Pomatias*), ear shell (abalone *Haliotis*) and terrestrial snail (*Helix*), the peristaltic wave travels in the tail-to-head direction. However in other creatures, the peristaltic wave moves in the head-to-tail direction, for example in leech, earthworm, eelworm (*Criconemoides*) and snake movement. Peristaltic biomimetic micro engineering systems have emerged in a diverse range of exciting applications including respiratory injury mitigation [31], soft robotics exploiting pliable pneumatic actuators [32]. Further applications include heart-lung devices, dialysis machines, blood filter machines and pneumatic self-re-inflating tyres in the automotive industry. Waldrop et al. [33] have presented a quantitative analysis on pumping by peristaltic hearts to identify physical constraints, focusing on the influence of Womersley number, compression frequency and compression ratio on flow and the energetic circulation costs. They showed that all flow characteristics were extremely sensitive to modifications in compression ratio but less sensitive to pulsatile effects (Womersley number and compression frequency). Kuijsters et al. [34] have scrutinized the dynamics of uterine peristalsis and fertility by uterine contractions, focusing on patients who have hormonally stimulated intervals. Ali et al. [35] analyzed the effects of conduit curvature on peristaltic pumping of viscoelastic bio-fluids in hemodynamics using a FTCS (forward time centred space) algorithm. Asghar et al. [36] used a finite element technique to simulate the micro-robotic swimming in a magneto-rheological flow through a deformable channel. Several novel bioinspired pumping flow models have also considered the combined effects of electroosmosis and peristaltic pumping. Bandopadhyay [37] have studied the influence of electrical (electroosmotic) body force on a single pulse peristaltic wave in a micro-channel, computing the spatial pressure difference and wall shear stress. This analysis was however confined to steady electroosmotic flow and propagating (peristaltic) wavy walls. A time-dependent analysis with asymmetry of the walls was presented by Narla et al. [38] wherein the effects of the phase difference, external electric axial field, and Debye length on the flow characteristics were evaluated in detail. Tanveer et al. [39] considered combined magneto hydrodynamic

and electroosmotic peristaltic pumping of third grade viscoelastic liquids in a micro-channel with slip effects. Tanveer et al. [40] further considered the electrokinetic peristaltic transport of viscoplastic fluids in a micro-conduit. Narla et al. [41] computed the electroosmotic peristaltic pumping flow in embryological tapered channel with asymmetric zeta potentials at the channel walls and a Jeffrey viscoelastic model, for a finite Debye layer.

In the present work, a unique pumping mechanism for electromagnetic bio microfluidics transport is studied which is a counterpart of the peristaltic mechanism. The current study deploys a different peristaltic pumping mechanism which is referred to as a *valveless pumping* mechanism which is induced by the rhythmic membrane contraction with compression and expansion phases. It is inspired by the natural pumping mechanism utilized in the micro-level transport of the fluids in the insect respiratory systems which were first examined for insect trachea physiology by Aboelkassem and Staples [42, 43]. They analyzed the selective pumping of fluids via the *periodic contraction cycle* of the distensible channel wall. Aboelkassem and Staples [44] further developed a comprehensive three-dimensional hydrodynamic propulsion model for this pumping mechanism in a micro-channel using lubrication theory. Subsequently, Krishnashischen and Staples [45] discussed the slip effects on non-propagative wall contraction, considering unidirectional net flow without external deformations. However, these studies were restricted to Newtonian fluids. Bhandari et al. [46] generalized the previous studies to consider non-Newtonian biofluids with a polar (couple stress) model in propagative membrane contraction through the micro-channel. Their study showed that larger couples stress parameter and membrane shape parameter are responsible for high-pressure gradient. In the context of propagative membrane motion, some further recent studies have been communicated by Tripathi et al. [18] who considered electro-osmosis in membrane pumping in a micro-channel and Bhandari et al. [47] who studied hydromagnetic membrane pumping in a micro-conduit.

An inspection of the scientific and technical literature has revealed that thus far the membrane pumping mechanism with electroosmosis effects in a micro-conduit (capillary) for bio microfluidics with electrical double layer effects has not been examined. This is a topic of great relevance to several emerging technologies including bio-fuel cells [48], electroosmotic pharmacodynamics [49], spinal rehabilitation electrokinetic micro-engineering [50] and smart micro-pumps in medical engineering [51] and soft robotic internal propulsion control [52]. A new electroosmotic insect-inspired pumping model is therefore developed in this article which focuses on the hydrodynamic mechanisms involved in the interaction of the electroosmosis flow with the membrane propagation in the micro-conduit. Pumping flow is developed by the double rhythmic wall contraction with expansion and compression i.e. the micro-pump transports

the fluid owing to wall deformation by virtue of membrane kinematics. Electroosmotic phenomena are simulated with the Poisson-Boltzmann equation. The impact of the membrane shape parameter is retained in the model. The effects of Helmholtz-Smoluchowski velocity (U_{HS}) and reciprocal of electrical double layer (EDL) thickness (κ) and additionally the membrane parameter on the pressure distribution, radial and axial velocity distribution, volumetric flow rate pumping characteristic, wall shear stress (WSS), and vector field streamline patterns are visualized graphically and interpreted at length.

2 Mathematical formulation

2.1 Geometry of the Problem

To simulate theoretically the hydrodynamics of induced electroosmotic flow due to the rhythmic wall contractions and electric body force in an axisymmetric micro-conduit, lubrication theory is deployed. The micro- tube is assumed to be a cylindrical with a very high aspect ratio (i.e., $\delta = R/L << 1$) and depicted below in Fig. 1.
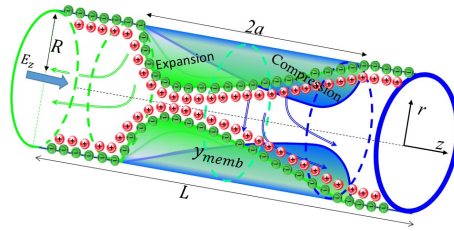
Fig. 1 Schematic of the membrane model in electroosmotic micro-conduit pumping.

2.2 Governing equations

Newtonian incompressible viscous ionic aqueous electroosmotic pumping in the presence of body force that is generated only as a result of the action of the applied electric field on the free ions within the electrical double layer (EDL) is considered. The relevant conservation equations (mass and momentum) may be written extending the earlier model of Aboelkassem [53] as follows:

$$\frac{\partial u}{\partial z} + \frac{1}{r}\frac{\partial(rv)}{\partial r} = 0, \tag{1a}$$

$$\frac{\partial u}{\partial t} + u\frac{\partial u}{\partial z} + v\frac{\partial u}{\partial r} = -\frac{1}{\rho}\frac{\partial p}{\partial z} + \nu\Big(\frac{\partial^2 u}{\partial z^2} + \frac{1}{r}\frac{\partial}{\partial r}\Big(r\frac{\partial u}{\partial r}\Big)\Big) + \frac{\rho_e}{\rho}E_z, \tag{1b}$$

$$\frac{\partial v}{\partial t} + u\frac{\partial v}{\partial z} + v\frac{\partial v}{\partial r} = -\frac{1}{\rho}\frac{\partial p}{\partial r} + \nu\Big(\frac{\partial^2 v}{\partial z^2} + \frac{\partial}{\partial r}\Big(\frac{1}{r}\frac{\partial(rv)}{\partial r}\Big) - \frac{u}{r^2}\Big) + \frac{\rho_e}{\rho}E_r, \tag{1c}$$

in the above equation ρ is the fluid density, $V = (u, v, 0)$ is a divergence-free velocity vector field $(\nabla \cdot V = 0)$ subject to the no-slip boundary conditions on the walls, p is the pressure, $E(= -\nabla\Phi)$ is the applied external electric field, ρ_e is the net charge density of the aqueous medium of permittivity ϵ, and Φ is the electric potential.

2.3 Potential distribution in electrokinetic phenomena

In an electrostatic theory, the electric potential Φ in the EDL that can be related to the charge density and is governed by the well-known Poisson equation as

$$\nabla^2\Phi = -\frac{\rho_e}{\epsilon}. \tag{2}$$

It is assumed that the ions are point charges (ρ_e) and the permittivity (ϵ) of the fluid is constant, the net electric-charge density in symmetric electrolyte solution can be obtained by the Boltzmann distribution as

$$\rho_e = -2zen_0(n_+ - n_-), \tag{3}$$

where e is the fundamental charge, z is the valence of the ions, n_0 is the bulk concentration, $n_\pm$ are the number of densities of cations and anions respectively. The Nernst-Planck equation in the absence of chemical reactions is given as (See Ref. [37]).

$$\frac{\partial n_\pm}{\partial t} = D_\pm \nabla^2 n_\pm + D_\pm \frac{ez}{k_B T}\nabla.(n_\pm \nabla\Phi) - \nabla.(n_\pm V), \tag{4}$$

where $D_\pm = k_B T m_\pm$ is the diffusivity in term of the mobility in the range $\sim 10^{-9} m^2/s$ (where, $m_\pm$ is the mobility). The relation between the applied electric field (E) and the electric field at the surface is illustrate through the expression $E << \kappa\zeta$. Typically, the EDL thickness is around $\kappa \sim 0.01 - 0.1\mu m$ and Zeta potential is approximate $\sim 10^{-2} V$. The potential of the applied electric field is nearby $E \sim 1k V/cm$. Therefore, It is assumed that the applied electric field is much weaker than the electric field within the electric double layer.

2.4 Lubrication theory

The flow conservation equations can be solved by employing lubrication theory. The viscous effect of a flow in the micro-scale regime is dominant. Hence, the assumption of very low Reynolds number assumption is valid. Consider the non-dimensional variables: $z' = z/L$, $r' = r/R$, $H' = H/R$, $t' = tU_0/L$, $u' = u/U_0$, $v' = v/(\delta U_0)$, $p' = pR^2/(\mu U_0 L)$, $\tau'_{rz} = \tau_{rz}R/(\mu U_0)$, $Q' = Q/(U_0 \pi R)$, $Re = \rho U_0 R/\mu$, $\phi' = ze\Phi/(k_B T)$, $U_{HS} = -\epsilon(k_B T/ze)E_z/(\mu U_0)$. τ is the shear stress, Q is the volumetric flow rate, Re is the Reynolds number, U_{HS} is the Helmholtz-Smoluchowski velocity and is a measure of the strength of the body force due to the applied electric field. The arbitrary reference velocity U_0 can be defined as Lf, where f denotes the membrane contractions frequency in

one time period T^*. Since in microfluidics applications $Re \sim 0.001 - 1.0$ and the geometry of micro-tube is characterized by a typical length scale $\sim \delta (= R/L) << 1$ so that the requirement of lubrication theory is satisfied. The conservation equations that govern electrokinetic membrane micro-tube flow problem after dropping primes in the above non-dimensional variables, using the balance of the terms $E_r : \delta E_z$, can be obtained as

$$\frac{\partial u}{\partial z} + \frac{1}{r}\frac{\partial (rv)}{\partial r} = 0, \tag{5a}$$

$$Re\delta\left[\frac{\partial u}{\partial t} + u\frac{\partial u}{\partial z} + v\frac{\partial u}{\partial r}\right] = -\frac{\partial p}{\partial z} + \left[\delta^2\frac{\partial^2 u}{\partial z^2} + \frac{\partial^2 u}{\partial r^2} + \frac{1}{r}\frac{\partial u}{\partial r}\right]$$
$$+ U_{HS}\left[\delta^2\frac{\partial^2 \Phi}{\partial z^2} + \frac{1}{r}\frac{\partial}{\partial r}\left(r\frac{\partial \Phi}{\partial r}\right)\right], \tag{5b}$$

$$Re\delta^3\left[\frac{\partial v}{\partial t} + u\frac{\partial v}{\partial z} + v\frac{\partial v}{\partial r}\right] = -\frac{\partial p}{\partial r} + \delta^2\left[\delta^2\frac{\partial^2 v}{\partial z^2} + \frac{\partial^2 v}{\partial r^2} + \frac{1}{r}\frac{\partial v}{\partial r} - \frac{v}{r^2}\right]$$
$$+ \delta^2 U_{HS}\left[\delta^2\frac{\partial^2 \Phi}{\partial z^2} + \frac{1}{r}\frac{\partial}{\partial r}\left(r\frac{\partial \Phi}{\partial r}\right)\right], \tag{5c}$$

The Nernst-Planck Eq. (4) in moving frame of reference using the non-dimensional parameter with dropping all the primes, takes the form

$$Pe\kappa^2\left(\frac{\partial n_\pm}{\partial t} + \nabla.(n_\pm V)\right) = \left(\kappa^2\frac{\partial^2 n_\pm}{\partial z^2} + \frac{1}{r}\frac{\partial}{\partial r}(r\frac{\partial n_\pm}{\partial r})\right) + \left(\kappa^2\frac{\partial}{\partial z}\left(n_\pm\frac{\partial \Phi}{\partial z}\right) + \left(\frac{1}{r}\frac{\partial}{\partial r}\left(rn_\pm\frac{\partial \Phi}{\partial r}\right)\right)\right) \tag{6}$$

$\kappa = (2z^2 e^2 n_0/\epsilon k_B T)^{1/2} R$ represents the inverse of the Debye length (λ_D); this indicates the penetration of the zeta potential at lower wall of the micro-tube into the bulk fluid. k_B is the Boltzmann constant and T is the absolute temperature. The Peclet number $Pe = U_0 L/D_\pm$ is in the range from $\sim 0.01 - 1$ for the typical values taken as $U_0 \sim 10^{-2} m/s$. The Nernst-Plank equation can be reduced for $\kappa- > 0$ and $\kappa^2 Pe- > 0$ as

$$\left(\frac{\partial^2 n_\pm}{\partial r^2} + \frac{1}{r}\frac{\partial n_\pm}{\partial r}\right) + \frac{1}{r}\frac{\partial}{\partial r}\left(rn_\pm\frac{\partial \Phi}{\partial r}\right) = 0, \tag{7}$$

subject to the bulk conditions $n_\pm(\Phi = 0) = 1$ and $\frac{\partial n_\pm}{\partial r} = 0$ where $\frac{\partial \phi}{\partial r} = 0$. This gives the Boltzmann distribution for the ions are

$$n_\pm = \exp(\mp\Phi). \tag{8}$$

The electric potential distribution due to the presence of the EDL is described by the Poisson-Boltzmann equation that can be obtained by combining equations (2), (3) and substituting the expression of $n_\pm$, the Poisson-Boltzmann equation can be obtained as:

$$\left(\frac{\partial^2 \Phi}{\partial r^2} + \frac{1}{r}\frac{\partial \Phi}{\partial r}\right) = \kappa^2 \sinh\Phi. \tag{9}$$

Electrokinetic Insect-Bioinspired Membrane Pumping in a High Aspect Ratio Bio-Microflui

The above non-linear equation can be linearized by expanding hyperbolic sin function on the right hand side of the equation (9) in Taylor series and discarding all terms that are quadratic or of higher order Φ, that led to linear equation is known as the Debye-Hückel approximation gives

$$\frac{\partial^2 \Phi}{\partial r^2} + \frac{1}{r}\frac{\partial \Phi}{\partial r} - \kappa^2 \Phi = 0, \tag{10}$$

Under lubrication approach, employing the stream function formulation ($u = (1/r)\partial\psi/\partial r$ and $v = -(1/r)\partial\psi/\partial z$) and eliminating pressure by cross differentiation, the reduced momentum equation are obtained as:

$$\frac{\partial}{\partial r}\left[\frac{1}{r}\frac{\partial}{\partial r}\left(r\frac{\partial}{\partial r}\left\{\frac{1}{r}\frac{\partial\psi}{\partial r}\right\}\right)\right] + U_{HS}\frac{\partial}{\partial r}\left(\frac{1}{r}\frac{\partial}{\partial r}\left\{r\frac{\partial\Phi}{\partial r}\right\}\right) = 0. \tag{11}$$

The corresponding boundary conditions are

$$\psi = \frac{Q_0(t)}{2} - \int_0^z h\frac{\partial h}{\partial t}ds, \ \frac{1}{r}\frac{\partial\psi}{\partial r} = 0, \Phi = \zeta, \quad \text{at} \quad r = h \tag{12a}$$

$$\psi = 0, \ \frac{\partial}{\partial r}\left(\frac{1}{r}\frac{\partial\psi}{\partial r}\right) = 0, \frac{\partial\Phi}{\partial r} = 0, \quad \text{at} \quad r = 0 \tag{12b}$$

here, $Q_0(t)$ is the volumetric flow rate at inlet of the membrane pipe.

3 Analytical solutions

From the equation (10) subject to the corresponding boundary conditions in the equation (12), the electric potential distribution is obtained as (See Ref. [54])

$$\Phi = \zeta\frac{I_0[\kappa r]}{I_0[\kappa h]}. \tag{13}$$

The stream function is determined by integrating (11) together with the remaining boundary conditions in the equation (12) and the solution of electric potential as in equation (13)

$$\psi = \frac{1}{16}\frac{\partial p}{\partial z}\left(r^4 - 2h^2 r^2\right) + U_{HS}\zeta\left(\frac{r^2}{2} - \frac{hI_0[\kappa r]}{\kappa I_0[\kappa h]}\right), \tag{14}$$

where $I_0[\kappa r]$ and $I_0[\kappa h]$ are modified Bessel function of the first kind and order 0. The velocity field is obtained from (14) as:

$$u = \frac{1}{4}\frac{\partial p}{\partial z}(r^2 - h^2) + U_{HS}\zeta\left(1 - \frac{I_0[\kappa r]}{I_0[\kappa h]}\right), \tag{15a}$$

$$v = \frac{1}{16}\frac{\partial^2 p}{\partial z^2}(2h^2 - r^2)r + \left(\frac{h}{4}\frac{\partial p}{\partial z}r - U_{HS}\zeta\frac{I_1[\kappa h]I_1[\kappa r]}{(I_0[\kappa h])^2}\right)\frac{\partial h}{\partial z}. \tag{15b}$$

Using equation (15b), one can extract a relationship between the motion of the membrane micro-tube wall and the axial pressure gradient $\partial p/\partial z$:

$$\frac{h^3}{16}\frac{\partial^2 p}{\partial z^2} + \frac{h^2}{4}\frac{\partial p}{\partial z}\frac{\partial h}{\partial z} - U_{HS}\zeta\frac{\partial h}{\partial z}\left(\frac{I_1[\kappa h]}{I_0[\kappa h]}\right)^2 = \frac{\partial h}{\partial t}. \tag{16}$$

Here, the axial pressure gradient is given by

$$\frac{\partial p}{\partial z} = \frac{1}{h^4}\left[G(t) + 16\int_0^z h\frac{\partial h}{\partial t}ds + 8U_{HS}\zeta h\left(h - \frac{2}{\kappa}\frac{I_1[\kappa h]}{I_0[\kappa h]}\right)\right]. \tag{17}$$

Integrating once yields

$$p(z,t) = p(0,t) + \int_0^z \frac{\partial p}{\partial z}(s,t)ds. \tag{18}$$

$G(t)$ is determined by evaluating (17) at $z = L$ and $\Delta p(t) = p(L,t) - p(0,t)$

$$G(t) = \frac{1}{\int_0^L h^{-4}dz}\left[\Delta p(t) - 16\int_0^L h^{-4}\left(\int_0^z h\frac{\partial h}{\partial t}ds + U_{HS}\zeta h\left\{\frac{h}{2} - \frac{1}{\kappa}\frac{I_1[\kappa h]}{I_0[\kappa h]}\right\}\right)dz\right]. \tag{19}$$

The non-dimensional flow rate is therefore given by

$$Q(z,t) = 2\int_0^h urdr = -\frac{1}{8}\frac{\partial p}{\partial z}h^4 - U_{HS}\zeta\left[h^2 - \frac{2h}{\kappa}\frac{I_1[\kappa h]}{I_0[\kappa h]}\right]. \tag{20}$$

Local wall shear stress is given by

$$\tau_w(z,t) = \left(\frac{\partial u}{\partial r}\right)_{r=h} = \frac{1}{2}\frac{\partial p}{\partial z}h - U_{HS}\zeta\kappa\frac{I_1[\kappa h]}{I_0[\kappa h]}. \tag{21}$$

4 RESULTS AND DISCUSSION

4.1 Propagative membrane contraction

The shape of the propagative membrane contraction at walls of the micro-tube as:

$$h(z,t) = \begin{cases} \frac{1}{2}; & if z \in [-\frac{1}{2}, -a)\bigcup(a, \frac{1}{2}], \\ \frac{1}{2} + r_{memb}(z,t); & if z \in [-a, a], \end{cases} \tag{22}$$

where a is a non-dimensional distance measured from the middle of a unity length tube (i.e., $a \in [-1/2,\ 1/2]$). The membrane profile is given as

$$r_{memb}(z,t) = 2\alpha_0\left(\left(\frac{z}{a}\right)^{2M} - 1\right)^3(1 - k_0z\cos(\pi t))\sin^2(\pi t). \tag{23}$$

The exponent $M = 1, \ 2, \ 3, \cdots$ controls the shape of the contraction profile, and the non-dimensional parameter. It is noted that the wall profile and its deformation are prescribed by the membrane kinematic play the important role in the present work. Here, the profile is a well-posed continuous function and does not suffer from any discontinuities when derivatives are needed. The sundry parameters (such as a, k_0, α_0, and M) are used to optimize in the membrane equations. Once the membrane profile is prescribed, all the flow quantities can be calculated.

4.2 parameter selection

For numerical calculations, the following parameters are prescribed for the membrane shape: $M = 2$, $a = 0.1$, $\alpha_0 = 0.225$, $k_0 = 9.95$. The typical values of other parameters are $\rho = 10^3 \ kg \ m^{-3}$, $\epsilon = 7.0832 \times 10^{-10} \ C/\mathbf{V}m$. The typical propagative membrane speed varies from a few $1mm/s$ to $10 \ cm/s$. The diameter of the tube is considered around $100 \ \mu m$ [18]. Lab-on-a-chip devices employing electroosmosis can usually employ electric fields of strengths $1 \ k\mathbf{V}/cm$ [41]. It may be noted here that these values are typically used in micro-scale applications [55, 56]. All computations are performed in MATLAB.

4.3 Electrokinetic effects and the induced flow field

In this sub-section, the variations in fluid characteristics such as pressure difference, velocity profile, shear stress and volumetric flow rate are evaluated for the effect of different electrokinetic parameters. The electrokinetic parameters studied are the inverse EDL thickness (κ), and the Helmholtz-Smoluchowski velocity (U_{HS}) respectively. The flow characteristic distributions are depicted in **Figs. 2-12**.

The effects of the Helmholtz-Smoluchowski velocity U_{HS} and inverse EDL thickness κ, on the pressure distribution are presented in **Figs. 2 & 3**. In **Fig. 2**, the distribution of the pressure along the tube length is computed for $U_{HS} = -1, \ 0 \ , 1$. Negative $U_{HS} = -\varepsilon(k_B T/ze)E_z/(\mu U_0)$ implies the axial electric field is in the positive z-direction (from the entry to the exit of the micro-tube) and positive U_{HS} corresponds to the reverse case i.e. axial electric field is in the negative z-direction (from the exit to the entry of the micro-tube). For $U_{HS} = 0$ electroosmotic effects are negated i.e. purely Newtonian membrane pumping is considered as studied in [53]. For a given inverse EDL thickness (κ) value, the global maximum (minimum) value of pressure distribution attained at $U_{HS} = 1$. In addition, $p(z,t)$ is positive for $U_{HS} = -1$ & 0 during the compression phase i.e. for (a) $t = T/4$ while it becomes *negative* value during the expansion phase for b) $t=3T/4$. Maximum pressure in the micro-tube is computed at $z = 0$ for $U_{HS} = 1$ in the compression phase whereas minimal pressure also arises at t= 0 for $U_{HS} = 1$ but in the expansion phase. Overall, a change in the direction of the axial electrical field produces pressure distribution results with opposite signs for the compression

and expansion phases. An increment in κ also strongly modifies the pressure magnitudes. Only the case of $U_{HS} = -1$ is studied i.e. axial electrical field is in the positive z direction. Pressure is strongly accentuated with rising values of κ (smaller values of EDL thickness) initially along the micro-tube and attains a peak during the compression phase at time $t=T/4$ (**Fig. 3a**); however thereafter the trends are reversed and larger $\kappa = (2z^2e^2n_0/\varepsilon k_B T)^{1/2}R$ (i.e. smaller EDL thickness) produces a strong downturn in pressures. Axial location (z-coordinate) therefore has an influence on $p(z,t)$ magnitudes even during the compression phase (**Fig. 3a**). Similar magnitude results are observed but again with opposite sign, during the expansion phase at time $t=3T/4$ [**Fig.3(b)**]. In this case there is an increase again in pressure for z< 0 with increment in κ (i.e. reduction in EDL thickness) but the magnitude is lower compared with the compression phase (**Fig. 3a**). The minimal pressure now arises for $z > 0$ again with the largest value of electroosmotic inverse EDL parameter, $\kappa = 10$ (least value of EDL thickness). The figures clearly capture the *periodic nature* of the membrane pumping.
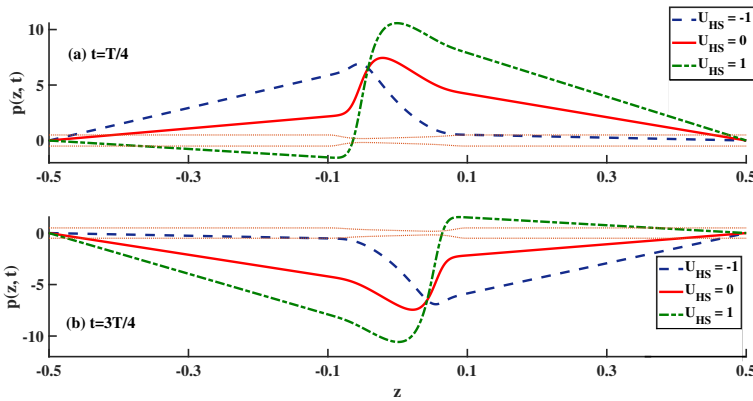
Fig. 2 Pressure distributions along the membrane micro-tube for different U_{HS} values with $\kappa = 5$ at (a) $t = T/4$, (b) $t = 3T/4$.
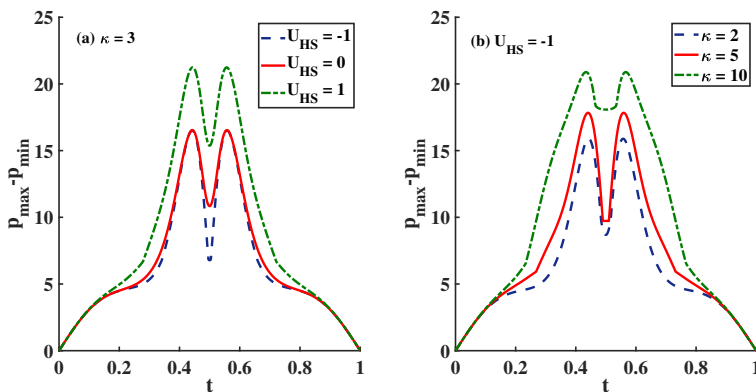
Maximum-to-minimum pressure differences ($P_{max} - P_{min}$) with time for various values of κ and U_{HS} is depicted in **Fig. 4(a-b).** Initially in **Fig. 4a**, with κ, ($P_{max} - P_{min}$) is enhanced from zero at $t = 0$, and achieves a first peak just before $t = 0.5$. At the stage of the transmission phase, oscillatory behaviour is clearly observed. With further progression in time, there is a dip in pressure and then a resurgence in maximum pressure after $t = 0.5$; following this the magnitude of ($P_{max} - P_{min}$) decays and tends to zero at $t = 1$. This result illustrates that the maximum pressure is produced during the compression phase both immediately before and after $t = 0.5$ which will significantly affect the flow rate. The case $U_{HS} = 1$ (reversed axial electrical field, E_z) attains maximum pressure difference whereas the case $U_{HS} = -1$
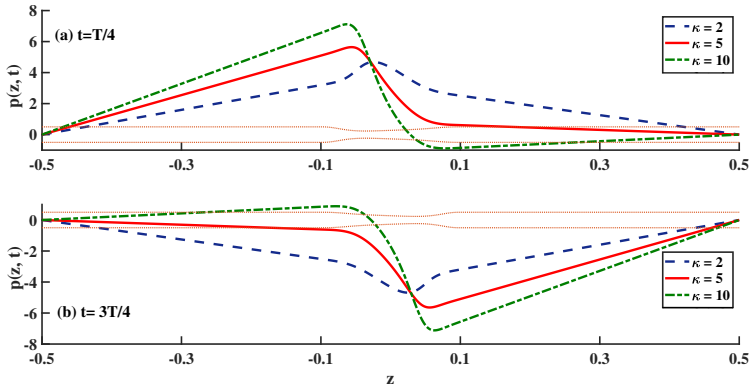
Fig. 3 Pressure distributions along the membrane micro-tube for different κ values with $U_{HS} = -1$ at (a) $t = T/4$, (b) $t = 3T/4$.

(aligned axial electrical field, E_z) generates the minimal pressure difference. The case $U_{HS} = 0$, i.e. vanishing electrical field produces $(P_{max} - P_{min})$ values between these other two cases. In **Fig. 4b**, for the case $U_{HS} = -1$ (aligned axial electrical field), an increment in inverse EDL parameter induces a significant boost in pressure difference $(P_{max} - P_{min})$. Again there are two peaks computed around $t = 0.5$. However unlike **Fig. 4a**, there is a significant plateau between the two peaks which is absent in **Fig. 4a**. This plateau is expanded with increment in κ. Subsequently, there is a strong depletion in pressure difference with further elapse in time. Similar pressure difference magnitudes are computed in both **Figs. 4a** and **b.**

The evolution in the axial velocity for different spatial position (z), Helmholtz-

Fig. 4 Maximum-to-minimum pressure differences in the membrane micro-tube during one period (a) for different U_{HS} values and (b) for different κ values.

Smoluchowski velocity (U_{HS}) and inverse EDL thickness parameter (κ), are presented in **Figs. 5-6**. The non-uniform axial velocity profile is clearly visible during the compression and expansion phase snapshots corresponding to $t = T/4$ & $3T/4$, respectively in **Fig. 5** for the case where no electrical double layer thickness is present (non-electrical) corresponding closely to the scenario studied in [53]. The maximum axial velocity is observed at the midway region i.e. along the micro-tube centre line, at axial position $z = -0.07$. **Fig. 6a** and **b** consider the *electroosmotic membrane pumping case,* and show that the magnitude of the axial velocity is positive for $U_{HS} = -1$ (reversed electrical field case for which $-U_{HS}\zeta\frac{\partial h}{\partial z}(\frac{I_1[\kappa h]}{I_0[\kappa h]})^2$ becomes positive in the axial pressure gradient Eq. (17) implying assistive i.e. favourable pressure gradient in the regime) while negative values (deceleration) are induced for $U_{HS} = 1$, (positive aligned electrical field case for which $-U_{HS}\zeta\frac{\partial h}{\partial z}(\frac{I_1[\kappa h]}{I_0[\kappa h]})^2$ stays negative and an adverse axial pressure gradient is present) as shown in **Fig. 5**. It is further noteworthy that the maximum and minimum axial velocity appear as sharp pulses and are not gradually attained owing to the nature of the compression/expansion membrane pumping mechanism.

The influence of κ is also depicted to enhance the axial velocity for the
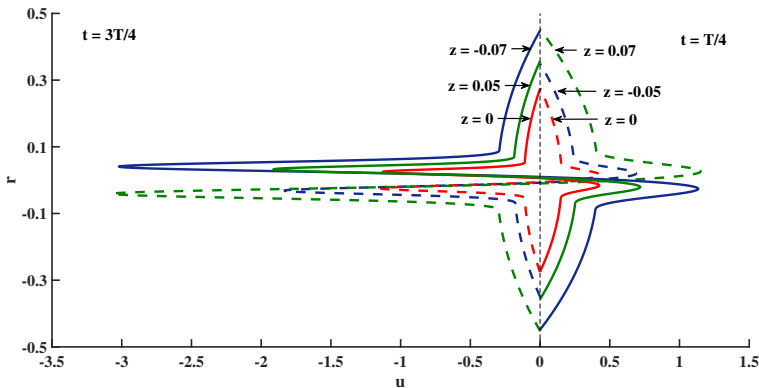
Fig. 5 Velocity profiles for different membrane cross sections with no EDL.

case $U_{HS} = -1$ (assistive axial electrical field), as shown in **Fig 6a** during the compression phase ($t = T/4$). Furthermore the *reverse axial flow* (negative values of axial velocity) observed at the lowest value of $\kappa = 2$ is eliminated with higher values of $\kappa = 5, 10$ indicating that a thinner electrical double layer stabilizes the electroosmotic flow. Conversely for the case $U_{HS} = 1$ (inhibiting axial electrical field), **Fig. 6b** indicates that a strong retardation in axial flow is generated with increment in inverse EDL thickness parameter (κ). Only for a limited region with minimal $\kappa = 2$, is acceleration computed in the axial flow. The implication is therefore that with aligned axial electrical field, a

decrease in electrical double layer thickness (EDL) is counter-productive and generates strong back flow in the micro-tube, which is the converse behaviour to that computed with reversed axial electrical field (**Fig. 6a**). The stability and sensitivity of the micro-tube axial flow to orientation of axial electrical field is therefore clearly established during the compression phase. In both cases the axial velocity vanishes at the micro-tube wall (maximum r value) in accordance with the classical *no-slip* condition imposed there.
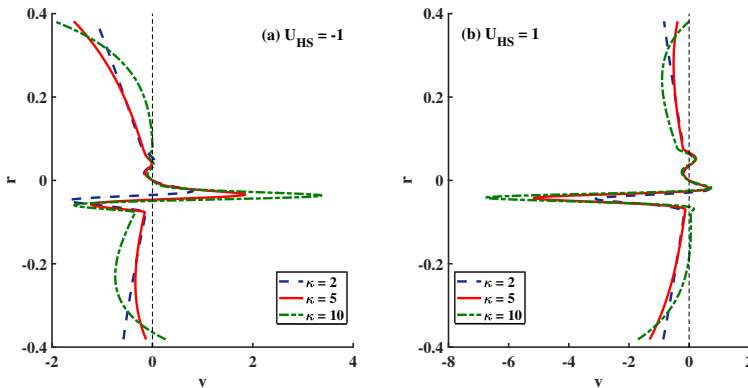
Figs. 7a,b illustrate the distribution in radial velocity (v) component again
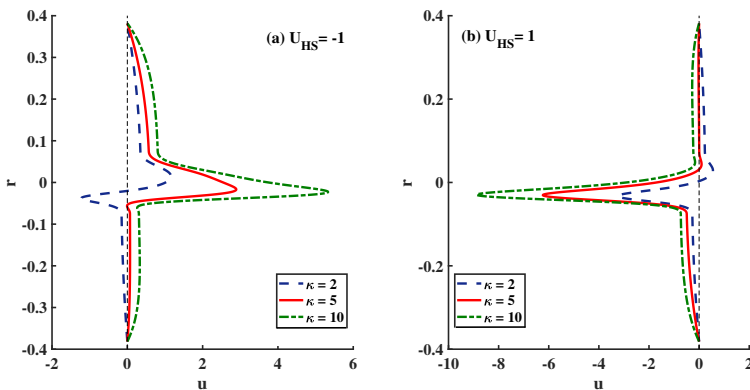
Fig. 6 Axial velocity profiles in the presence of EDL at time $t = T/4$ and at cross section $x = a/2$ for (a) $U_{HS} = -1$ (b) $U_{HS} = 1$.

at different spatial positions (z), Helmholtz-Smoluchowski velocity (U_{HS}) and inverse EDL thickness parameter κ. There is a fluctuation in radial velocity with radial coordinate and generally negative values are computed for both $U_{HS} = 1$ and $U_{HS} = -1$ scenarios. Initially for $U_{HS} = -1$, radial velocity is damped at the periphery of the tube (near the wall) and thereafter it is gradually increased attaining a peak value at the centre line, with increment in inverse EDL thickness parameter (κ). This is observed at the upper values of radial coordinate (**Fig. 7a**). However for negative r there is a substantial deceleration in transverse flow with greater values of κ. For $U_{HS} = 1$, (**Fig. 7b**) again for the compression phase $t = T/4$ a much more prominent decrease in radial velocity is computed with larger values of inverse EDL thickness parameter (κ) i.e. thinner electrical double layer thickness generally strongly decelerates the radial flow, with the minimum computed again at the centre line for $\kappa = 10$. However a very weak acceleration arises but is constrained to close proximity to the centre line in the core flow for $\kappa = 10$. Significant manipulation in the transverse flow is therefore achieved with adjustment in the thickness of the electrical double layer which in turn is related to the charge mobility at the inner micro-tube surface [56] and can also be modified with the membrane pumping (compression).

**Fig. 8** depicts the distribution in volumetric flow rate (Q) (corresponding to

Fig. 7 Radial velocity profiles in the presence of EDL at time $t = T/4$ and at cross section $x = a/2$ for (a) $U_{HS} = -1$ (b) $U_{HS} = 1$.

the axial flow), with axial coordinate, z, i.e. along the micro-tube length for various values of κ & U_{HS}. **Fig. 8a** shows that for $U_{HS} = -1$ (assistive axial electrical field case where E_z is in the negative z-direction), the volumetric flow rate is increased strongly with progression along the micro-tube. However there is a step change around $z = 0$ and two plateaus are computed with a much larger magnitude in the second. In the first plateau, a constant increase in Q is induced with increment in inverse EDL thickness parameter κ and magnitudes are smaller. The same is observed in the second group of plateaus with much greater magnitudes. However in between a very strong linear enhancement arises around $z = 0$. Clearly the reduction in EDL thickness with larger κ markedly increases the pumping efficiency and generates strong axial volume flow rates, which are desirable in bio microfluidics operations. The reverse trends are observed for $U_{HS} = 1$ (inhibiting axial electrical field case where E_z is in the positive aligned z-direction), the volumetric flow rate is increased strongly with an upsurge in inverse EDL thickness parameter, κ. However, the same step change and general increase with axial coordinate is computed for volumetric flow rate. There is therefore a delicate interplay between spatial location (which aids flow rate enhancement) and axial electrical field and electrical double layer thickness (EDL) which can either boost or deplete the flow rate, depending on the orientation of the electrical field in the micro-tube. These require careful prescription to achieve the desired effects in ==electrokinetic== membrane pumping devices (especially during the compression phase) [4] where either acceleration or deceleration may be necessary depending on the application considered.

Figs. 9 and 10 illustrate the distributions of wall shear stress (WSS) for
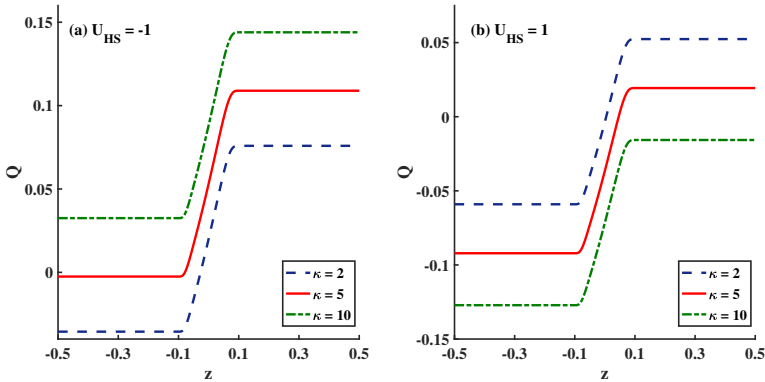
Fig. 8 Volume flow rate in the presence of EDL at time $t = T/4$ for (a) $U_{HS} = -1$ (b) $U_{HS} = 1$.

different time stages and combinations of U_{HS} and κ values. Wall shear stress attains a peak in the membrane region during the compression and expansion phase at time $t = T/4$ & $3T/4$, respectively. In **Fig. 9a**, the wall shear stress is accentuated with an increment in U_{HS} in the vicinity of the membrane and remain constant away from that region. The wall shear stress is flipped (**Fig. 9b**) in the negative direction for $U_{HS} = -1$. Moreover **Figs. 10a,b** reveal that for both the compression and expansion phases in the micro-tube membrane pumping, an elevation in κ (i.e. reduction in EDL thickness) however, suppresses the magnitude of wall shear stress for a fixed value of $U_{HS} = -1$ (reversed axial electrical field case). From these results, it is evident that the *positive* value of Helmholtz-Smoluchowski velocity is responsible for substantially elevating the wall shear stress i.e. inducing acceleration at the micro-tube internal surface whereas negative value of Helmholtz-Smoluchowski velocity in conjunction with larger EDL thickness parameter are found to markedly damp the wall shear stress (deceleration at the micro-tube internal surface).

Finally, **Figs. 11-12** visualize the stream function contour plots for different values of U_{HS} and κ during the compression phase ($t = T/4$). These figures show that the contour lines behave in a similar fashion with different axial electrical field directions ($U_{HS} = -1$, $U_{HS} = 1$) and also in absence of electrical field ($U_{HS} = 0$). The streamlines are however of greater magnitude towards the *backward direction* during the contraction phase, whereas maximum contour lines toward the *forward direction* are computed during the expansion phase. These results illustrate that the membrane kinematic generates the flow inside the micro-tube in both directions. In the absence of the Helmholtz-Smoluchowski velocity ($U_{HS} = 0$), the contour lines attained both +ve and -ve values. However, with *non-zero* Helmholtz-Smoluchowski velocity ($U_{HS} = -1$ & 1) electroosmotic body force plays an important role
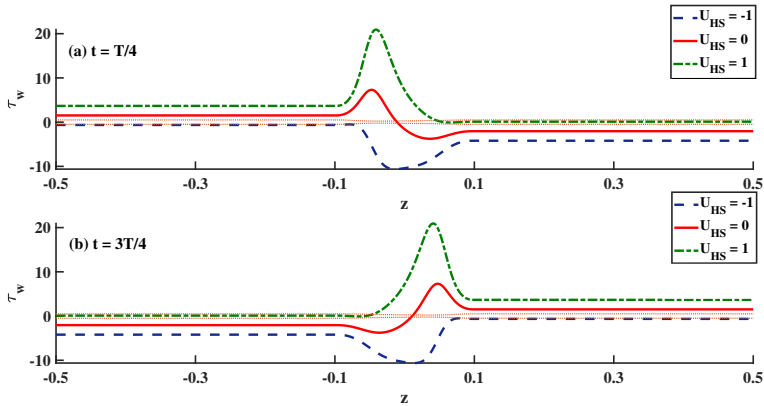
Fig. 9 Wall shear stress distribution for different values of U_{HS} with $\kappa = 5$ for (a) $t = T/4$ (b) $t = 3T/4$.
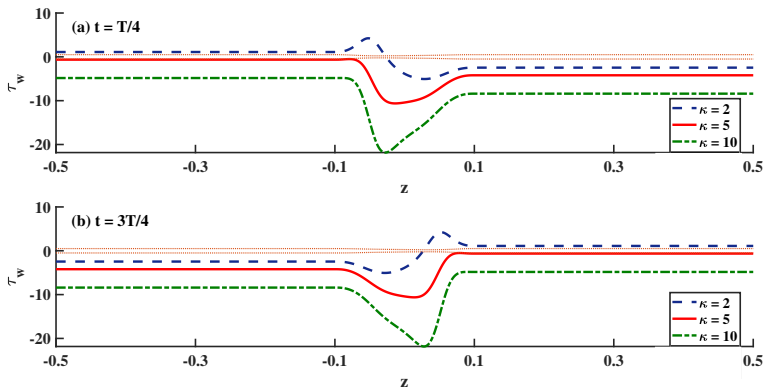

Fig. 10 Wall shear stress distribution for different values of κ with $U_{HS} = -1$ for (a) $t = T/4$ (b) $t = 3T/4$.

in changing the flow direction as observed in **Figs. 11a   b**. This result illustrates that the flow field is primarily orientated in the *backward* direction for $U_{HS} < 0$ whereas *forward flow* generated by $U_{HS} > 0$. **Figs. 12(a & b)** indicate that increment in inverse EDL thickness (κ) produces negative values for the stream function contours. The magnitude is fixed near the range of (-1, -9) for the highest value of κ. Moreover, the contour lines are clustered near the micro-tube wall at maximum value of κ. Thus flow structure is strongly modified in the vicinity of the micro-tube wall with greater κ or with decrease in electrical double layer thickness.
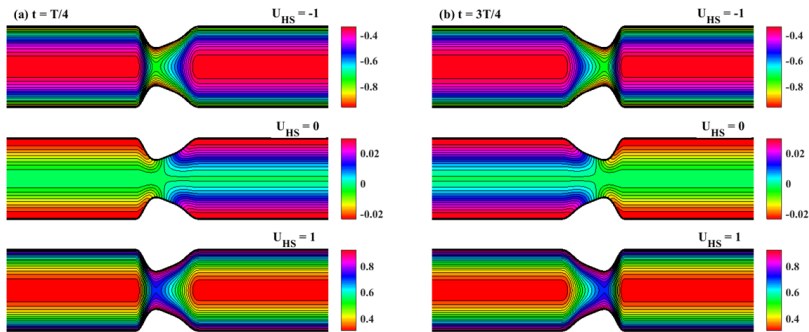
Fig. 11 Stream lines of velocity vector during the (a) compression phase (b) expansion phase for different values of U_{HS}.
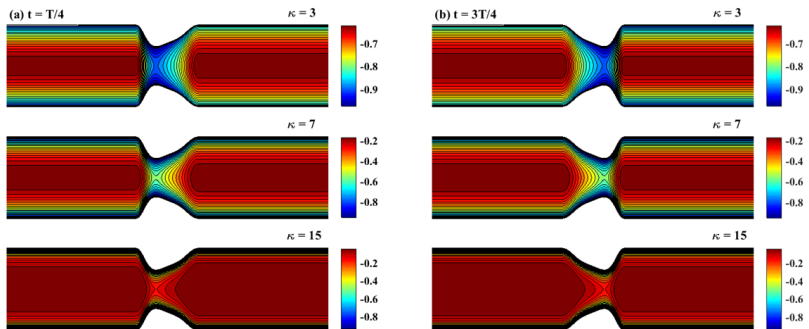
Fig. 12 Stream lines of velocity vector during the (a) compression phase (b) expansion phase for different values of κ.

5 CONCLUSIONS

Motivated by emerging applications in bio microfluidics devices, an electrokinetic bio-inspired microfluidics pumping model has been developed using lubrication theory and insect-inspired membrane kinematics. A low Reynolds number approach has been deployed for a high aspect ratio micro-tube with an axisymmetric viscous Newtonian ionic flow. The membrane attached to the

wall performs periodic compression and relaxation phases during the complete contraction cycle. Thus, the micro-pump transports the fluid owing to wall deformation by virtue of membrane kinematics. Electroosmotic phenomena are simulated with the Poisson-Boltzmann equation. The impact of the membrane shape parameter is retained in the model. The model is non-denationalized with appropriate scaling transformations. Analytical solutions are derived. The effects of Helmholtz-Smoluchowski velocity (U_{HS}) and reciprocal of electrical double layer (EDL) thickness (κ) on the pressure distribution, radial and axial velocities distribution, volumetric flow rate pumping characteristic, wall shear stress (WSS), and vector field streamline patterns are computed using MATLAB and visualized graphically. The main findings of the present simulations may be summarized as follows:

1. The maximum axial velocity is computed at the centre line of the micro-tube at fixed position, $z = -0.07$. The magnitude of the axial velocity is positive for Helmholtz-Smoluchowski velocity $U_{HS} = -1$ (positive direction of axial electrical field) whereas negative values are computed for $U_{HS} = 1$ (reversed direction of axial electrical field).

2. Initially for $U_{HS} = -1$, radial velocity is damped in the compression phase at the periphery of the tube (near the wall) and thereafter it is gradually increased attaining a peak value at the centre line, with increment in inverse EDL thickness parameter (κ). For $U_{HS} = 1$, *again for the compression phase* ($t = T/4$), a much more prominent decrease in radial velocity is observed with a boost in values of inverse EDL thickness parameter (κ).

3. A boost in wall shear stress accompanies an increment in positive U_{HS} in the vicinity of the membrane micro-tube wall. The wall shear stress is reversed (back flow) for negative $U_{HS} = -1$ (i.e. reverse electrical field case).

4. Volumetric flow rate (Q) and wall shear stress are elevated with increment in κ (i.e. thinner EDL), for a fixed value of U_{HS}.

5. Pressure along the tube length, $p(z, t)$ is positive for $U_{HS} = -1$ & 0 during the compression phase ($t = T/4$), whereas it becomes negative during the expansion phase ($t = 3T/4$). Elevation in the pressure is also produced with increment in κ during the compression phase with the opposite trend observed during the expansion phase At the transmission phase stage, an *oscillation* is computed for the pressure difference, $P_{max} - P_{min}$.

6. Streamline contours indicate that the flow field in the micro-tube is orientated in the *backward* direction for $U_{HS} < 0$ whereas *forward flow* is generated by $U_{HS} > 0$.

7. The contraction of the membrane motion has a strong impact on the wall shear stress and pressure gradient profiles. The axial pressure gradient attains similar topologies during the compression phase at time ($t = 3T/4$) and expansion snapshot time $t = T/4$ but with opposite sign.

The present simulations have revealed some intriguing trends in hydrodynamic characteristics of membrane-based micro-tube pumping inspired by an alternative insect-inspired rhythmic mechanism, of relevance to electroosmotic bio microfluidics. However, attention has been confined to Newtonian flows.

Author's Contributions

All authors contributed equally to this work. The authors read and approve the manuscript.

Informed consent

All authors declare that they have no competing interest.

Ethical approval

The paper reflects the authors' own research and analysis in a truthful and complete manner.

FUNDING ACKNOWLEDGEMENT

References

[1] Mariella, R.: Sample preparation: the weak link in microfluidics-based biodetection. Biomedical microdevices **10**(6), 777–784 (2008)

[2] Burklund, A., Zhang, J.X.: Microfluidics-based organism isolation from whole blood: an emerging tool for bloodstream infection diagnosis. Annals of biomedical engineering **47**(7), 1657–1674 (2019)

[3] Zhang, L., Srinivasakannan, C., Li, S., He, Y., Chen, K., Yin, S., *et al.*: Mixing performance in t-shape microchannel at high flow rate for villermaux-dushman reaction. Microchemical Journal **155**, 104662 (2020)

[4] Au, A.K., Lai, H., Utela, B.R., Folch, A.: Microvalves and micropumps for biomems. Micromachines **2**(2), 179–220 (2011)

[5] Rosenfeld, T., Bercovici, M.: Dynamic control of capillary flow in porous media by electroosmotic pumping. Lab on a Chip **19**(2), 328–334 (2019)

[6] Buch, J.S., Wang, P.-C., DeVoe, D.L., Lee, C.S.: Field-effect flow control in a polydimethylsiloxane-based microfluidic system. Electrophoresis **22**(18), 3902–3907 (2001)

[7] Kusama, S., Sato, K., Yoshida, S., Nishizawa, M.: Self-moisturizing smart contact lens employing electroosmosis. Advanced Materials Technologies **5**(1), 1900889 (2020)

[8] Farooqi, A.R., Bader, R., van Rienen, U.: Numerical study on electrome-chanics in cartilage tissue with respect to its electrical properties. Tissue Engineering Part B: Reviews **25**(2), 152–166 (2019)

[9] Fong, K., Boey, M., Koh, W., Feng, P.: Cytokine concentrations in the synovial fluid and plasma of rheumatoid arthritis patients: correlation with bony erosions. Clinical and experimental rheumatology **12**(1), 55–58 (1994)

[10] Vacikova, A.: Assessment of electrophoretic mobilities of some human isoamylases. Journal of Chromatography A **69**(2), 349–354 (1972)

[11] Faraji, A.H., Jaquins-Gerstl, A.S., Valenta, A.C., Weber, S.G.: Electroki-netic infusions into hydrogels and brain tissue: Control of direction and magnitude of solute delivery. Journal of neuroscience methods **311**, 76–82 (2019)

[12] Sasaki, N., Kitamori, T., Kim, H.-B.: Ac electroosmotic micromixer for chemical processing in a microchannel. Lab on a Chip **6**(4), 550–554 (2006)

[13] Cheng, I.-F., Yang, H.-L., Chung, C.-C., Chang, H.-C.: A rapid elec-trochemical biosensor based on an ac electrokinetics enhanced immuno-reaction. Analyst **138**(16), 4656–4662 (2013)

[14] Song, Y., Chen, P., Chung, M.T., Nidetz, R., Park, Y., Liu, Z., McHugh, W., Cornell, T.T., Fu, J., Kurabayashi, K.: Ac electroosmosis-enhanced nanoplasmofluidic detection of ultralow-concentration cytokine. Nano letters **17**(4), 2374–2380 (2017)

[15] Narla, V., Tripathi, D.: Electroosmosis modulated transient blood flow in curved microvessels: study of a mathematical model. Microvascular research **123**, 25–34 (2019)

[16] Tanveer, A., Salahuddin, T., Khan, M., Malik, M.Y., Alqarni, M.: Theo-retical analysis of non-newtonian blood flow in a microchannel. Computer Methods and Programs in Biomedicine **191**, 105280 (2020)

[17] Tripathi, D., Jhorar, R., Borode, A., Bég, O.A.: Three-layered electro-osmosis modulated blood flow through a microchannel. European Journal of Mechanics-B/Fluids **72**, 391–402 (2018)

[18] Tripathi, D., Narla, V., Aboelkassem, Y.: Electrokinetic membrane pump-ing flow model in a microchannel. Physics of Fluids **32**(8), 082004 (2020)

[19] Hlushkou, D., Kandhai, D., Tallarek, U.: Coupled lattice-boltzmann and

finite-difference simulation of electroosmosis in microfluidic channels. International journal for numerical methods in fluids **46**(5), 507–532 (2004)

[20] Harnett, C.K., Templeton, J., Dunphy-Guzman, K.A., Senousy, Y.M., Kanouff, M.P.: Model based design of a microfluidic mixer driven by induced charge electroosmosis. Lab on a Chip **8**(4), 565–572 (2008)

[21] Bég, O.A., Rashidi, M., Rastegari, M., Bég, T.A., Motsa, S., Halim, A.: Dtm-padé numerical simulation of electrohydrodynamic ion drag medical pumps with electrical hartmann and electrical reynolds number effects. Journal of Advanced Biotechnology and Bioengineering **1**(2), 62–79 (2013)

[22] Pan, W., Daily, M., Baker, N.A.: Numerical calculation of protein-ligand binding rates through solution of the smoluchowski equation using smoothed particle hydrodynamics. BMC biophysics **8**(1), 1–12 (2015)

[23] Bég, O.A., Hameed, M., Bég, T.A.: Chebyshev spectral collocation simulation of nonlinear boundary value problems in electrohydrodynamics. International Journal for Computational Methods in Engineering Science and Mechanics **14**(2), 104–115 (2013)

[24] Gogoi, A., Reddy, K.A., Mondal, P.K.: Electro-osmotic flow through nanochannel with different surface charge configurations: A molecular dynamics simulation study. Physics of Fluids **33**(9), 092115 (2021)

[25] Song, F., Zhang, L., Chen, R., Liu, Q., Liu, J., Yu, J., Liu, P., Duan, J., Wang, J.: Bioinspired durable antibacterial and antifouling coatings based on borneol fluorinated polymers: Demonstrating direct evidence of antiadhesion. ACS Applied Materials & Interfaces **13**(28), 33417–33426 (2021)

[26] Fan, J.-B., Luo, J., Luo, Z., Song, Y., Wang, Z., Meng, J., Wang, B., Zhang, S., Zheng, Z., Chen, X., *et al.*: Bioinspired microfluidic device by integrating a porous membrane and heterostructured nanoporous particles for biomolecule cleaning. ACS nano **13**(7), 8374–8381 (2019)

[27] Manzoor, N., Bég, O.A., Maqbool, K., Shaheen, S.: Mathematical modelling of ciliary propulsion of an electrically-conducting johnson-segalman physiological fluid in a channel with slip. Computer methods in biomechanics and biomedical engineering **22**(7), 685–695 (2019)

[28] Nima, N.I., Ferdows, M., Anwar Bég, O., Kuharat, S., Alzahrani, F.: Biomathematical model for gyrotactic free-forced bioconvection with oxygen diffusion in near-wall transport within a porous medium fuel cell. International Journal of Biomathematics **13**(04), 2050026 (2020)

Electrokinetic Insect-Bioinspired Membrane Pumping in a High Aspect Ratio Bio-Microflui...

[29] Feher, J.J.: Quantitative Human Physiology: an Introduction vol. 2. Academic press, ??? (2017)

[30] Alexander, R.M.: Exploring Biomechanics vol. 40. Distributed by WH Freeman, ??? (1992)

[31] Song, J.W., Paek, J., Park, K.-T., Seo, J., Huh, D.: A bioinspired microfluidic model of liquid plug-induced mechanical airway injury. Biomicrofluidics **12**(4), 042211 (2018)

[32] Chen, F., Dirven, S., Xu, W., Li, X.: Soft actuator mimicking human esophageal peristalsis for a swallowing robot. IEEE/ASME Transactions on Mechatronics **19**(4), 1300–1308 (2013)

[33] Waldrop, L.D., He, Y., Battista, N.A., Neary Peterman, T., Miller, L.A.: Uncertainty quantification reveals the physical constraints on pumping by peristaltic hearts. Journal of the Royal Society Interface **17**(170), 20200232 (2020)

[34] Kuijsters, N.P.M., Methorst, W.G., Kortenhorst, M.S.Q., Rabotti, C., Mischi, M., Schoot, B.C.: Uterine peristalsis and fertility: current knowledge and future perspectives: a review and meta-analysis. Reproductive biomedicine online **35**(1), 50–71 (2017)

[35] Ali, N., Javid, K., Sajid, M., Anwar Bég, O.: Numerical simulation of peristaltic flow of a biorheological fluid with shear-dependent viscosity in a curved channel. Computer methods in biomechanics and biomedical engineering **19**(6), 614–627 (2016)

[36] Asghar, Z., Ali, N., Sajid, M., Anwar Bég, O.: Micro-organism swimming propulsion through a shear rate-dependent biorheological fluid in an active channel assisted by a magnetic field. J Magn Magn Mater **486**, 165283 (2019)

[37] Bandopadhyay, A., Tripathi, D., Chakraborty, S.: Electroosmosis-modulated peristaltic transport in microfluidic channels. Physics of Fluids **28**(5), 052002 (2016)

[38] Narla, V., Tripathi, D., Sekhar, G.: Time-dependent analysis of electroosmotic fluid flow in a microchannel. Journal of Engineering Mathematics **114**(1), 177–196 (2019)

[39] Tanveer, A., Mahmood, S., Hayat, T., Alsaedi, A.: On electroosmosis in peristaltic activity of mhd non-newtonian fluid. Alexandria Engineering Journal **60**(3), 3369–3377 (2021)

[40] Tanveer, A., Khan, M., Salahuddin, T., Malik, M.: Numerical simulation

of electroosmosis regulated peristaltic transport of bingham nanofluid. Computer methods and programs in biomedicine **180**, 105005 (2019)

[41] Narla, V.K., Tripathi, D., Anwar Bég, O.: Electro-osmosis modulated viscoelastic embryo transport in uterine hydrodynamics: mathematical modeling. Journal of biomechanical engineering **141**(2) (2019)

[42] Aboelkassem, Y., Staples, A.E.: Flow transport in a microchannel induced by moving wall contractions: a novel micropumping mechanism. Acta Mechanica **223**(3), 463–480 (2012)

[43] Aboelkassem, Y., Staples, A.E.: A bioinspired pumping model for flow in a microtube with rhythmic wall contractions. Journal of Fluids and Structures **42**, 187–204 (2013)

[44] Aboelkassem, Y., Staples, A.E.: A three-dimensional model for flow pumping in a microchannel inspired by insect respiration. Acta Mechanica **225**(2), 493–507 (2014)

[45] Chatterjee, K., Staples, A.: Slip flow in a microchannel driven by rhythmic wall contractions. Acta Mechanica **229**(10), 4113–4129 (2018)

[46] Bhandari, D., Tripathi, D., Narla, V.: Pumping flow model for couple stress fluids with a propagative membrane contraction. International Journal of Mechanical Sciences **188**, 105949 (2020)

[47] Bhandari, D., Tripathi, D., Narla, V.: Magnetohydrodynamics-based pumping flow model with propagative rhythmic membrane contraction. The European Physical Journal Plus **135**(11), 1–19 (2020)

[48] Singh, R., Kaur, N., Singh, M.: Bio-compatible bio-fuel cells for medical devices. Materials Today: Proceedings **44**, 242–249 (2021)

[49] Faraji, A.H., Jaquins-Gerstl, A.S., Valenta, A.C., Ou, Y., Weber, S.G.: Electrokinetic convection-enhanced delivery of solutes to the brain. ACS Chemical Neuroscience **11**(14), 2085–2093 (2020)

[50] Hale, C., Yonan, J., Batarseh, R., Chaar, R., Jonak, C.R., Ge, S., Binder, D., Rodgers, V.G.: Implantable osmotic transport device can reduce edema after severe contusion spinal cord injury. Frontiers in bioengineering and biotechnology, 806 (2020)

[51] Ramsey, R., Ramsey, J.: Generating electrospray from microchip devices using electroosmotic pumping. Analytical Chemistry **69**(6), 1174–1178 (1997)

[52] Kim, S., Laschi, C., Trimmer, B.: Soft robotics: a bioinspired evolution in

robotics. Trends in biotechnology **31**(5), 287–294 (2013)

[53] Aboelkassem, Y.: Pumping flow model in a microchannel with propagative rhythmic membrane contraction. Physics of Fluids **31**(5), 051902 (2019)

[54] Riad, A., Khorshidi, B., Mansouri, A., Sadrzadeh, M.: Transient electroosmotic-driven ionic current magnetic fields in a charged nano-capillary. Colloids and Surfaces A: Physicochemical and Engineering Aspects **628**, 127374 (2021)

[55] Wang, T., Kleiven, S., Li, X.: Influence of anisotropic white matter on electroosmotic flow induced by direct current. Frontiers in Bioengineering and Biotechnology, 736 (2021)

[56] Li, D.: Electrokinetics in Microfluidics vol. 2. Elsevier, ??? (2004)